Interactions of a Transmembrane Helix and a Membrane: Comparative Simulations of Bacteriorhodopsin Helix A

Martin B. Ulmschneider,[†,‡] D. Peter Tieleman,[§] and Mark S. P. Sansom*[,†]

Laboratory of Molecular Biophysics, Department of Biochemistry, University of Oxford, South Parks Road, Oxford, OX1 3QU, United Kingdom, and Department of Biological Sciences, University of Calgary, 2500 University Drive NW, Calgary, AB T2N 1N4, Canada

Received: December 22, 2003; In Final Form: April 22, 2004

Helix A of bacteriorhodopsin was simulated by using molecular dynamics both in isolation and as part of the complete protein. A POPC lipid bilayer and an octane monolayer were used as model membranes. Comparison of various systems showed octane to be a good alternative to lipid bilayer membranes providing fast equilibration, increased sampling, and decreased computational cost. Similarly single-helix simulations were found to capture some of the details of the full-protein simulations. In particular, aromatic side chains were found to anchor in identical conformations in all simulations, regardless of the absence of a lipid−water interface or the remainder of the protein. Simulations displayed a remarkable robustness with respect to simulation parameters and system set up.

Introduction

Bacteriorhodopsin (BR) is one of the most intensively studied membrane proteins and has been the subject of many structural studies (as reviewed by, e.g., ref 1). There are currently 49 entries for BR X-ray and electron microscopy structures in the protein database (www.rcsb.org), more than for any other single membrane protein. Bacteriorhodopsin therefore provides an ideal system on which to test membrane protein simulation methods and protocols. For example, aspects of lipid/protein interactions were explored in a landmark use of molecular dynamics simulations to study the individual transmembrane α-helices of BR within a lipid bilayer environment.[2,3]

Many computational studies of bacteriorhodopsin have concentrated on mechanistic aspects.[4−11] In contrast, the current study is focused on the conformational dynamics of helix A from BR and its interactions with a membrane and a membrane mimetic environment. Molecular dynamics (MD) simulations provide a useful tool to study transmembrane (TM) helix domains from membrane proteins.[2,12−17]

MD simulations of isolated TM helices from membrane proteins are in part motivated by the two-state model of membrane protein folding,[18] which suggests that TM α-helices are independently stable in lipid bilayers.[19] This model implies that MD simulations may provide insights into the structure and stability of single TM helices isolated from more complex membrane proteins. The ability of the individual helices of BR to form independently stable TM α-helices has been the subject of numerous experimental studies.[18−24] For example, in a recent study[25] the structure of each of helices A to F in isolation when dissolved in DMSO was determined by NMR. Helices A to F were all found to form helices closely resembling those found in the crystal structures of the intact BR molecule.

Studies by Woolf and colleagues[2,3] have investigated in some detail the behavior of the individual bacteriorhodopsin helices via MD simulations. Surrounding each helix by 12 dimyristoylphosphatidylcholine (DMPC) lipids in a hexagonal unit cell it was possible explore differences in protein/lipid interaction energies, hydrogen-bonding patterns, and secondary structural stability. Helix A was found to be particularly stable and hence represents a good system to compare different membrane environments.

It has long been suggested that amphipathic aromatic amino acid side chains (i.e. tryptophan and tyrosine) play an important role in anchoring membrane proteins into their transbilayer environment.[26,27] This has been investigated by simulation studies on the interaction of indole with lipid bilayers[28,29] and by analysis of known structures of membrane proteins.[30,31] There have also been extensive studies of model TM helix peptides containing interfacial tryptophan residues, using both experimental[32,33] and computational[34] approaches. Bacteriorhosopsin provides a good test system to explore such interactions in a complex membrane protein as it contains 6 interfacial tryptophan and 7 interfacial tyrosine residues.

In the current study we exploit improvements in computer power to perform ∼15× longer simulations than those previously performed for helix A[2,3] in systems with ∼10× more lipid molecules. This enables us to achieve improved statistical sampling and to more closely approximate in vitro and in vivo studies in which the lipid:protein ratio is much higher than in the earlier simulations. In the current study, MD simulations of helix A have been performed in various membrane and membrane mimetic environments. Differences in simulation protocols have also been explored. The results are also compared with the simulated behavior of helix A within an intact BR molecule. In particular, we focus on the sampling of conformational space by helix A within these simulations, and on the interaction of the aromatic residues within helix A with its simulated environment.

* To whom correspondence should be addressed. Phone: +44 (0)1865 275371. Fax: +44 (0)1865 275182. E-mail: mark.sansom@biop.ox.ac.uk.
† University of Oxford.
‡ Current address: Department of Chemistry, University of Rome "La Sapienza", Piazzale Aldo Moro 5, Roma, I-00185 Italy.
§ University of Calgary.

10.1021/jp0379650 CCC: $27.50 © 2004 American Chemical Society
Published on Web 06/04/2004

TABLE 1: Simulations of Helix A[a]

system name	membrane	water	simulation box dimens $x \times y \times z$ [nm^3]	total atoms
small octane	278	3556	$5 \times 5 \times 7.5$	13149
large octane	388	8358	$5.3 \times 6.7 \times 10.2$	28435
vacuum		0	$5 \times 5 \times 7.5$	257
water		5797	$5 \times 5 \times 7.5$	17648
84 POPC	84 POPCs	3072	$5.3 \times 5.5 \times 7.3$	13841
128 POPC	128 POPCs	6435	$5.4 \times 6.8 \times 9.9$	26218
BR octane	558	15776	$7.5 \times 7.5 \times 8.6$	35512
BR POPC	266	9591	$8.0 \times 10.1 \times 10.7$	63511
heavy & dummy	same as small octane			13149
octane Ewald	same as small octane			13149
truncated termini	same as small octane			13145
84 POPC flipped	same as 84 POPC			13841
water Ewald	same as water			17648

[a] All simulations were of 10-ns duration (after 1 ns equilibration during which the protein atoms were restrained) except for water and water Ewald, which were both 5 ns. The last four simulations investigate different parameters for the above environments. In the octane Ewald and water Ewald systems the particle mesh Ewald[48] method was used to calculate long-range electrostatic interactions, the other simulations employing a 1.8-nm cutoff.

Methods

Overview of the Simulations. Helix A was extracted from the ground state 1cwq structure[35] (resolution of 0.225 nm). The sequence used in the simulations was Ac-Pro^8-Glu^9-Trp^{10}-Ile^{11}-Trp^{12}-Leu^{13}-Ala^{14}-Leu^{15}-Gly^{16}-Thr^{17}-Ala^{18}-Leu^{19}-Met^{20}-Gly^{21}-Leu^{22}-Gly^{23}-Thr^{24}-Leu^{25}-Tyr^{26}-Phe^{27}-Leu^{28}-Val^{29}-Lys^{30}-Gly^{31}-Met^{32}-Gly^{33}-CONH$_2$. Thus, helix A is formed by a largely hydrophobic core, which is flanked by two aromatic and one charged residue at each end and is ~3.3 nm in length. In the truncated termini system the neutral acetyl and amide groups were replaced by a positively charged N-terminus and a negatively charged C-terminus, respectively.

Helix A was simulated in a range of different simulations environments, as summarized in Table 1. The POPC and Octane simulations explore Helix A spanning a phospholipid bilayer and a membrane mimetic octane slab, respectively. The BR simulations provide a comparison of the behavior of Helix A in isolation with a simulation of an intact (monomeric) BR molecule. Control simulations of Helix A in vacuo and in water were also performed, in addition to a number of simulations to explore the effects of choice of helix termini, treatment of long-range electrostatics, and of initial helix conformation as well as a time-saving approximation to the force field.

System Preparation. *Octane Slab.* To assemble a bilayer mimetic octane slab, Helix A was inserted in a box along with a mixture of randomly positioned octane and water molecules. The protein atoms were harmonically restrained and a 1 ns equilibration simulation run (at 300 K) during which the *x* and *y* box dimensions were fixed. During the first 0.2 ns the octane forms a uniform slab around the helix, expelling virtually all water molecules. Any water molecules trapped in the membrane near the protein were removed after 0.2 ns. The system was then equilibrated for a further 0.8 ns.

POPC Bilayer. The helix was inserted into a preequilibrated POPC bilayer as described in previous papers.[36,37] After inserting helix A the system was minimized and equilibrated for 1 ns at 300 K with harmonic restraints on the protein to retain its initial conformation, while allowing the lipids and water molecules to relax around it.

Water. Helix A was solvated with SPC (simple point charge) water. A box of similar dimensions to the small octane system was chosen. The system was minimized and equilibrated for 1 ns at 300 K with harmonic restraints on the protein.

Bacteriorhodopsin Monomer. The simulations of intact BR are described in more detail elsewhere.[38] Briefly, the ground-state BR molecule from the 1cwq structure was embedded in either an octane slab or a POPC bilayer, using the procedures described above. Ionization states of BR side chains were adjusted to match published experimental data and pK_A calculations.[39] The retinal was parametrized by using the GROMOS96 force field. The partial charges were derived from the results of ab initio calculations,[40] modified to meet the GROMACS charge group criterion.

Simulation Protocols. All simulations used GROMACS version 2.0 [41] (www.gromacs.org). The GROMOS96 43a2 force field[42] as implemented in GROMACS and the SPC water model[43] were used. For lipids parameters were taken from ref 44. An electrostatic twin-range cutoff of 0.8/1.4 nm and 1.0/1.8 nm was used for octane and lipid bilayer systems, respectively. The van der Waals cutoff was 1.4 nm in both cases. Simulations were run with a 2 fs integration time-step and neighbor lists were updated every 10 steps. Water, octane, POPC, and protein were each coupled separately to a heat bath with a temperature of 300 K and time constant $\tau_T = 0.1$ ps, using a Berendsen thermostat.[45] For the octane systems the compressibility in *x* and *y* was set to zero (i.e. fixed box size in *x* and *y*) and the pressure in the *z* direction was kept at 1.0 bar, using weak pressure coupling with time constant $\tau_P = 1.0$ ps and compressibility $\kappa_z = 4.6 \times 10^{-5}$ bar^{-1}. The POPC simulations were performed by using isotropic pressure coupling with compressibility $\kappa_{xyz} = 4.6 \times 10^{-5}$ bar^{-1} and time constant $\tau_P = 1.0$ ps. Bond lengths were constrained with LINCS.[46]

The "heavy & dummy" simulation was performed by using the heavy and dummy options for hydrogens.[47] The heavy hydrogen option increases the weight of the water hydrogen atoms by a factor of 4 while decreasing the weight of the oxygen to 12 atomic mass units. This removes the fast vibrational modes in the motion of water molecules. The dummy atom method distributes the force on protein hydrogens over the neighboring heavy atoms. The positions of the hydrogens themselves are reconstructed every step assuming an ideal geometry. This effectively removes the degrees of freedom involving the hydrogen atoms, while still generating correct forces and pressure for the system as a whole. Thus the integration time-step can be increased to 5 fs nearly halving the CPU time. Due to the longer time-step the neighbor list was updated every 3 steps for this simulation.

One simulation each of the water and the small octane systems was repeated by using the Ewald summation to treat long-range interactions as implemented in the particle mesh Ewald (PME) algorithm.[48,49] Short-range cutoffs for the real space part were chosen at $r_{Coul} = r_{vdW} = 0.9$ nm and the Fourier grid spacing for the reciprocal sum, interpolation order, and Ewald tolerance were chosen to be 0.12 nm, 4, and 10^{-5}, respectively. All other simulation parameters were kept the same.

Essential Dynamics Analysis. The sampling of conformational space was investigated by essential dynamics analysis.[50,51] First the eigenvectors for the C_α motions of helix A for all different simulations were calculated. Then the eigenvectors were sorted according to decreasing eigenvalues. Taking the first *n* eigenvectors describing 90% of the motion of a trajectory A, the overlap in eigenvectors with a different trajectory B was computed. This was done by calculating how many eigenvectors of simulation B are necessary to achieve a 90% overlap with the *n* eigenvectors, describing 90% of the motion for simulation

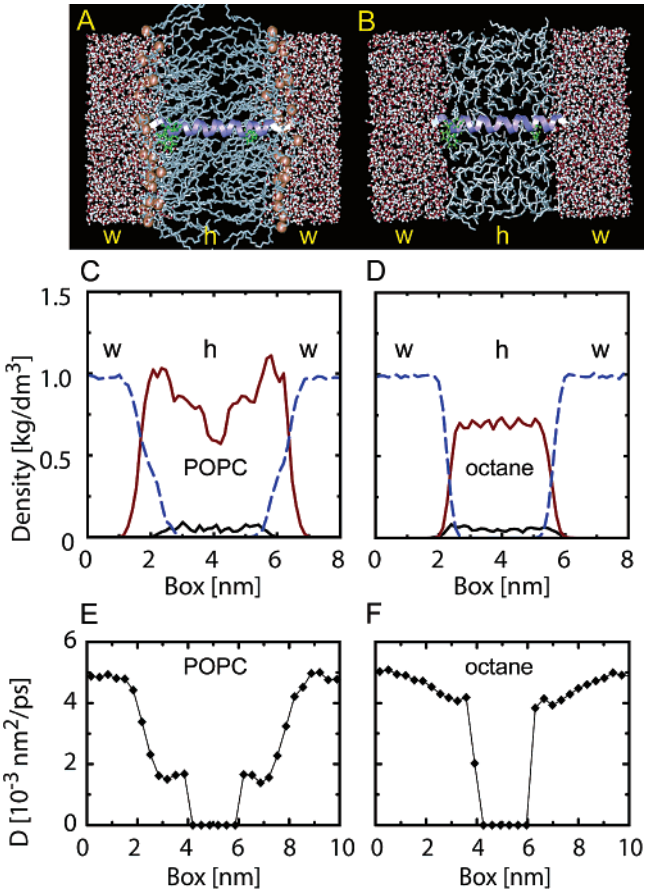

Figure 1. Lipid bilayer vs octane slab. Bacteriorhodopsin helix A (blue ribbon) is shown spanning (A) a POPC bilayer and (B) an octane slab, respectively. The water (w) and hydrophobic core (h) regions are labeled and in panel A the interface region is indicated via the phosphorus atoms (shown as large bronze spheres). The corresponding density profiles (averaged over the last 800 ps of the equilibration run) of the system components (broken blue line = water, red line = lipid or octane, black line = protein) are shown in panels C and D. In panels E and F the water diffusion coefficients are shown as a function of distance along the membrane perpendicular for the POPC and octane systems, respectively. Error bars have been omitted for clarity but range between 1% and 7%. (The values for panels E and F were from the larger simulation systems.)

A. Generally the eigenvalues of the system are a steeply declining function of the eigenvector index and the first few eigenvectors (ordered with respect to decreasing eigenvalue) usually represent most (80−90%) of the motion in a trajectory.[52]

Results

Structure and Dynamics. *Density and Diffusion Profiles.* The octane and POPC systems are shown in Figure 1, alongside the corresponding density profiles. The overall density profiles are similar in terms of the width and average density of their hydrophobic core regions. Similarly, in both systems the helix lies such that it spans the hydrophobic core symmetrically. The hydrophobic core region is composed of the fatty acyl tails of the lipid molecules, roughly corresponding to the space between the glycerol regions of each monolayer. For most bilayers this region has a width of ∼3.0 nm, and this is the case for the POPC bilayer used in these studies (see Figure 1C).

However, the octane slab provides a relatively narrow interfacial region (width <0.5 nm) while the POPC bilayer has an interfacial region of thickness ∼1.5 nm, in agreement with experimental estimates.[53] The wider interfacial region in POPC can be seen as a greater degree of overlap between the lipid and water density profiles than is seen for the octane and water density profiles. The differences in nature and size of the interfaces in the two systems provides us with a tool with which to probe in some detail how, e.g., aromatic residues behave at a water/membrane interface.

We also examined the dynamics of water molecules close to the interface, in terms of the diffusion coefficients for water molecules as a function of the membrane normal *z* (Figure 1E,F). The same overall pattern is seen in both systems, with a decrease in *D* at the interface. However, in the case of POPC the decrease is somewhat more pronounced, reflecting the existence of the more substantial interfacial region, where lipid headgroups and water molecules coexist. In summary, these results suggest that the octane slab is a reasonable approximation of a lipid bilayer, and that helix A orients itself in a similar fashion in the two environments.

Sampling of Conformational Space. Before proceeding to more detailed analysis it is important to consider how effectively our simulations sample possible conformations of helix A, and the conformational stability of helix A in the different simulations.

In Table 2 we compare the root-mean-square deviation (RMSD) from the initial structure for the different simulations. Comparing the simulations with one another, the smaller system simulations (small octane and 84 POPC) have a lower RMSD than the larger systems (large octane and 128 POPC). All four single helix simulations have much higher RMSD values (∼0.2 to 0.3 nm) than the RMSD between the different X-ray structures (0.04 nm). There is a general trend such that single helix MD > intact protein MD > X-ray with respect to the RMSDs. Furthermore, octane systems in general exhibit a higher RMSD than lipid bilayer systems. Thus we may conclude that the inherent flexibility of helix A is restricted within the intact protein by packing interactions with the remainder of the protein and, to a lesser extent, by the viscosity of the bilayer environment.

We have estimated a helix kink angle as a global measure of the internal distortion of helix A. In the X-ray structures the

TABLE 2: Summary of Simulation Results[a]

system name	Cα RMSD [nm]	tilt [deg]	kink [deg]	α-helicity [residues]
small octane	0.23 ± 0.03	28.8 ± 7.0	12.0 ± 7.0	20.9 ± 0.7
large octane	0.32 ± 0.09	25.8 ± 9.9	27.3 ± 14.7	20.4 ± 0.9
84 POPC	0.17 ± 0.03	28.2 ± 6.1	14.4 ± 5.1	23.5 ± 0.8
128 POPC	0.27 ± 0.04	11.2 ± 6.4	26.3 ± 9.8	22.8 ± 1.2
Ewald octane	0.30 ± 0.07	23.8 ± 8.8	20.9 ± 9.1	21.1 ± 0.6
heavy & dummy	0.24 ± 0.03	28.7 ± 8.5	13.3 ± 8.0	20.8 ± 0.7
truncated termini	0.21 ± 0.05	17.8 ± 7.8	20.5 ± 9.1	21.0 ± 0.6
84 POPC flipped	0.19 ± 0.03	28.9 ± 6.8	15.2 ± 6.6	23.6± 0.7
vacuum	0.20 ± 0.06	-	20.4 ± 11.6	21.5 ± 1.0
BR octane	0.10 ± 0.02	31.1 ± 4.0	12.2 ± 5.9	22.8 ± 0.6
BR POPC	0.09 ± 0.02	28.4 ± 3.8	10.5 ± 4.2	21.5 ± 0.6
X-ray structures[b]	0.04 ± 0.02	24.0 ± 1.0	6.9 ± 1.0	21.0 ± 1.3

[a] Tilt angles of α-helices were determined by least-squares fitting a straight line to the backbone atoms of the helix and calculating the angle between the fitted line and the membrane normal. Kink angles of helices were calculated by least-squares fitting two lines to the backbone atoms of the first 11 residues and last 11 residues of the helix and taking the angle between the two lines as the kink angle. The tilt of helix A from the crystal structured was measured with respect to an aligned bacteriorhodopsin structure (using the method of alignment described previously[30]). [b] The entries for the X-ray data represent the means for helix A from 22 crystallographic structures available in the RCSB. The Cα RMSD was averaged over the entire simulation time.

kink angle is relatively small (~7°), indicating that the helix is essentially unkinked. In contrast, in both the simulations of the intact protein and of the isolated helix A there is an increase in kink angle. This may be related to the presence of three glycine residues within the interior of helix A, which offers the possibility of some helix backbone flexibility. Indeed, the general trend in flexibility observed in terms of kink angle is the same as that for RMSDs, i.e., single helix MD > intact protein MD > X-ray.

A simple measure of the orientation of helix A with respect to the membrane is provided by the helix tilt angle averaged over the duration of each simulation. There are some variations in tilt angles between the simulations (analyzed in more detail below). Overall, the single helix simulation tilt angles are broadly similar to those for the intact protein and for the X-ray structures of the protein, and in turn these values are close to the average tilt angle for TM helices in membrane protein structures.[54,30] Note that the slightly higher tilt value of helix A in the BR octane simulation probably reflects the overall tilt of the complete BR molecule, which is ~16° for BR octane, ~14° for BR POPC, and ~12° for the aligned X-ray structure.

We also assessed helix A stability vs simulation conditions via analysis of the secondary structure of the helix. Thus, in Table 2 we include the mean length of the helical segment for the various simulation environments. Comparison of internal hydrogen-bonding patterns between the various simulations using DSSP[55] showed no significant differences between the simulations. Helix A remains stable in all membrane simulations and as expected shows a predominantly α-helical secondary structure. The single-helix octane simulations, however, displayed a slight loss of helicity at the C-terminus while the N-terminus stays helical throughout the simulations. In the 128 POPC simulation and very briefly in the large octane system Gly9 acts as a pivot for kinking, which resulted in loss of helicity at that residue. The most stable systems are the 84 and 128 POPC simulations with virtually no loss of helicity in any of the residues. All simulations have α-helical content values within the range of the X-ray structures.

Simulations in water showed partial unfolding between the third and fourth nanosecond around the Gly9 residue in the N-terminal half of the helix with subsequent stabilization in a horseshoe-like shape. In all other simulations the helix remained stable, including in vacuum. However, Gly9 acted as a pivot for kinking in most of the other simulations. Repeating the water simulation using Ewald sums rather than cutoff to calculate the long-range forces yielded similar results. The dynamics of the unfolding is slightly different and the system does not stabilize in the horseshoe shape. This caused an increased flexibility about the Gly9 pivot resulting in a slightly lower number of helical residues of 16.9 ± 3.5.

Generally it can be concluded that the choice of simulation parameters seems to have little effect on the secondary structure and stability of the helix relative to the choice of environment (i.e. water vs membrane model), which has a much more pronounced effect.

Essential Dynamics Analysis. The motion of helix A was analyzed for essential dynamics. This allows determination of the minimum number of eigenvectors necessary to describe 90% of the motion of the Cα atoms of helix A for a given environment. Almost twice (~20) as many eigenvectors are required to describe the motion in the simulations of the intact bacteriorhodopsin simulations compared to simulations of isolated helix A (for which ~10 eigenvectors are needed). The number of eigenvectors may be taken as a measure of the complexity of the motion of helix A. If twice as many eigenvectors are required to represent the motion of helix A, the interaction of the helix with its environment can be thought of as "more complicated". Interestingly the larger single-helix simulations (large octane and 128 POPC) required somewhat fewer eigenvectors to sample 90% of their Cα motion than did the smaller systems.

TABLE 3: Eigenvector Analysis[a]

	simulation *j*					
simulation *i*	small octane	large octane	84 POPC	128 POPC	BR octane	BR POPC
small octane	-	28	33	32	54	53
large octane	20	-	27	28	47	51
84 POPC	20	21	-	20	53	52
128 POPC	22	20	18	-	52	51
BR octane	50	45	51	52	-	19
BR POPC	55	46	51	49	21	-

[a] This shows the number of eigenvectors of a simulation *i* needed to achieve a 90% overlap with the eigenvectors representing 90% of the motion of simulation *j*. The matrix is not symmetric because it calculates a partial overlap (i.e. 90%) with respect to the "essential motion" (i.e. 90% of the RMSD) of another simulation. In each simulation this essential motion takes a different distribution along the eigenvectors of that simulation (i.e. different eigenvalues and a different number of eigenvectors representing 90% of the motion). Thus symmetry in the matrix means that the simulations are very similar in their eigenvalue distribution along their eigenvectors (i.e. they not only have similar eigenvectors for their essential motion but also similar eigenvalues along those eigenvectors).

To compare the difference in the motions between the various simulations the overlap of the eigenvectors was calculated. From the results in Table 3 we can extract several general trends. First, if we compare the two intact BR simulations we see good overlap of the eigenvectors describing the motions of helix A in the two simulations. For example, of the 20 eigenvectors that sample 90% of the motion of the BR POPC simulation, only 19 are necessary to sample 90% of the motion of the 18 eigenvectors that sample 90% of the motion of the BR octane simulation. Conversely 21 eigenvectors of BR octane are needed to achieve a 90% overlap with the 20 eigenvectors of the BR POPC system. This suggests that octane as a membrane mimetic for BR simulations provides comparable sampling of nanosecond time scale motions to POPC.

In the case of the single helix A simulations there is a little less overlap between, e.g., the motion in the POPC simulations and the motion in the octane simulations. However, the lowest degree of overlap is reserved for between the single-helix and intact bacteriorhodopsin simulations. This indicates that there are substantial influences of the remainder of the protein on the motion of helix A. This is not unexpected as about half the residues of helix A are in contact with the remainder of the protein, thus reducing helix flexibility in simulations of the intact protein. Overall, the essential dynamics suggests that there is a reasonable degree of overlap in conformational dynamics between independent simulations of a single TM helix in similar environments (e.g. small vs large octane), but that increasingly complex environments (i.e. POPC and the intact BR molecule) result in increasingly complex motions. Hence to attempt to understand such motions multiple comparative simulations are needed.

Helix Tilt and Kink. The helix tilt angle distributions reveal the overall orientation of helix A relative to the bilayer. As can be seen from, e.g., Figure 2, there is a clear difference between the small and large POPC simulation systems. The small system (84 POPC) shows tilt angles between 20° and 40° with respect

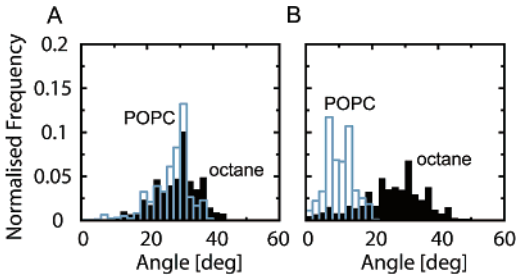

Figure 2. Helix tilt angle distributions. (A) The small octane (filled black bars) and 84 POPC systems (empty blue bars) systems are compared. (B) The large octane (filled black bars) and 128 POPC systems (empty blue bars) systems are compared.

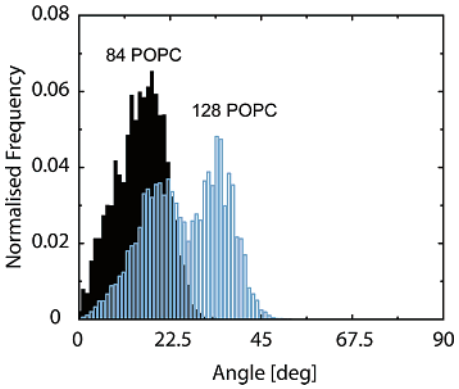

Figure 3. Helix kink angle distributions for the 84 POPC (filled black bars) and 128 POPC (empty blue bars) bilayer systems. The distributions from the small octane and large octane systems respectively are quite similar.

to the membrane normal, in contrast with the 128 POPC simulation for which only tilt angles between 0° and 20° are sampled. Both octane systems show larger mean tilt angles. The truncated termini simulation (in which the terminal amino and acid groups are charged) shows a lower tilt angle. Overall, this behavior indicates that both the system size and the nature of the membrane mimic may influence the behavior of the helix.

Distributions of the helix kink angles (Figure 3) exhibit a qualitatively similar behavior. The small octane (small octane, heavy & dummy, Ewald octane) systems show kink angles between 0° and 30°, with a peak around 10°. Again the simulation with the truncated termini is an exception with a broader peak centered around 20° and a range of kink angles from 0° to 50° (data not shown). The 84 POPC and the 84 POPC flipped bilayer simulations have identical kink angle distributions with angles between 0° and 20° and a peak at 18°. The large octane system shows the same 0° to 30° peak as the small octane simulations but has an additional peak between 30° and 40°. The 128 POPC bilayer simulation also has two peaks in its kink angle distribution, one near 18° and another between 30° and 40° similar to the large octane system.

On first thought it seems that the small systems have one state near 18°, while the large systems have an additional peak between 30° and 40°. The pivot for helix A kinking is the Gly9 residue for all simulations. However, the kinked states between 30° and 40° for the large octane system are actually due to a slight unfolding at the C-terminus of the helix. It therefore has similar kink angles but a different pivot. This means that only the 128 POPC simulation has an additional larger kinked state between 30° and 40°. Nevertheless, the less kinked state is identical in all simulations.

Generally it seems that small systems have kink angles between 0° and 30° while large systems have an additional stronger kinked state. This may be because smaller membranes have an increased rigidity as a consequence of the periodic boundary conditions. For tilt angles the conclusions are similar, while all small systems have tilt distributions between 20° and 40°, the large systems sample a significant number of states between 0° and 20°. In the case of the 128 POPC simulation these are the only states sampled. The simulation using heavy hydrogen and dummy atoms gives the same peaks as the small octane system for both tilt and kink angles.

Interactions at the Membrane/Water Interface. *Aromatic Ring Orientations.* It has been suggested that aromatic residues at the interfacial regions of the membrane act as anchors, locking the protein into the bilayer through interaction with the polar lipid headgroups.[26−29,32,33,56] Indeed there is strong evidence for the existence of so-called "aromatic belts" at the protein surface of the interfacial regions.[30] Recent simulations suggested that aromatic side chains located at the membrane/water interface may have preferred orientations.[57] The simulations of helix A described above provide an opportunity to explore the behavior of aromatic side chains at the membrane/water interface in more detail. In particular we focus on residues Trp3 at the N-terminus and Tyr19 at the C-terminus of helix A. These may be expected to help stabilize helix A in a membrane both in the isolated TM helix during protein folding and in the intact BR molecule. In contrast to these two residues, residues Trp5 and Phe20 are buried within the intact BR molecule and thus unlikely to play a role in protein stabilization in a bilayer. We therefore will not consider Trp5 and Phe20 any further.

Trp3. Residue Trp3 is located at the N-terminal interfacial region of helix A. In the X-ray structure the mean initial θ angle (defined in Figure 4) is ∼120° with 20 out of the 22 X-ray structures having angles between 100° and 130°. Figure 4 shows that the small and large octane systems exhibit similar behavior with a slight preference for the initial state around 120°. However, they allow "flipping" of Trp3 back and forth between 40° and 130°, roughly a 90° ring flip. The truncated octane simulation shows better separation of the two states, one at 120° and one at 40°, while the heavy & dummy simulation only samples the initial state at 120°, suggesting that the interaction of the hydrogens on the aromatic ring might be important for the orientation of aromatic side chains.

The comparable ring angle distributions for the POPC simulations are shown in Figure 5. Both the 84 and 128 POPC lipid bilayer simulations remain in the initial state at ∼120°. The 128 POPC system moves only briefly (for ∼0.5 ns) away from this conformation. To investigate whether the lack of the state at 40° in the POPC systems is due to the time scale of the motion or due to an unfavorable interaction with the lipids, the conformation at 40° was taken from the octane simulation and reinserted into the 84 POPC bilayer using the same protocol described above. This simulation shows the state to be stable for 10 ns with no flipping back into the original state occurring. Thus the interactions at the POPC/water interface of Trp3 seem to be substantially more long-lasting than those at an octane/water interface.

The high surface accessibility of Trp3 (61%) in the X-ray structure allows a meaningful comparison of the θ angles between simulations of helix A with the complete bacteriorhodopsin in a membrane. Interestingly, the BR POPC simulation (Figure 5D) shows the same orientation for the Trp3 as the 84 and 128 POPC simulations of the single helix A.

Time scales for the "flipping" transition range from 20 to 250 ps. On average nine flips per simulation were recorded in octane with none occurring in any of the POPC simulations.

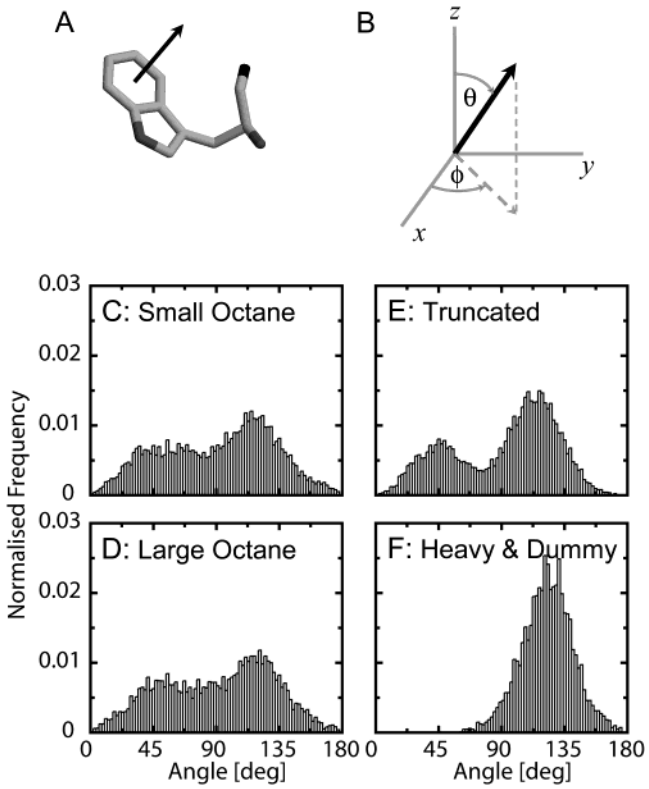

Figure 4. Distribution of the aromatic ring polar θ angles for residue Trp3 in the octane simulations. The aromatic plane normal has two angles θ (with respect to the z-axis) and φ (in the x,y plane) in the polar coordinate system. Parts A and B define the aromatic ring angles θ and φ in spherical polar coordinates. The simulations, as defined in Table 1, are as follows: (C) small octane; (D) large octane; (E) truncated termini; and (F) heavy & dummy.

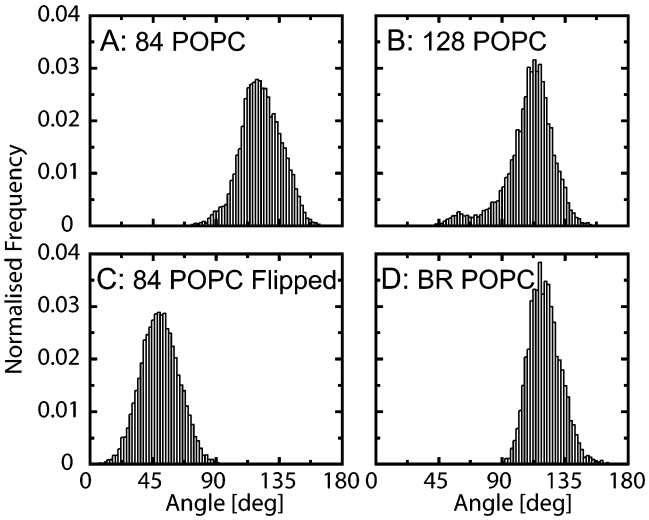

Figure 5. Distribution of the aromatic ring polar θ angles for residue Trp3 in the POPC simulations. The simulations, as defined in Table 1, are the following: (A) 84 POPC; (B) 128 POPC; (C) 84 POPC flipped; and (D) BR POPC.

This is an important difference between the two membrane models. In Figure 6 we show two conformations at 40° (t = 8114 ps) and 130° (t = 8139 ps) of Trp3 in the small octane simulation respectively as well as the intermediate states during the transition. The NH group forms hydrogen bonds with water molecules for the octane systems and both water and lipid headgroups for the POPC systems. The latter H bonds may be responsible for the restriction on ring flipping in the POPC simulations.

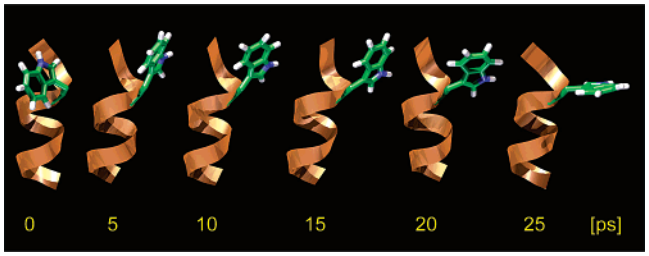

Figure 6. Successive snapshots from the small octane simulation showing the ring of Trp3 "flipping" at the interface. Only the N-terminal half of the helix is shown for clarity.

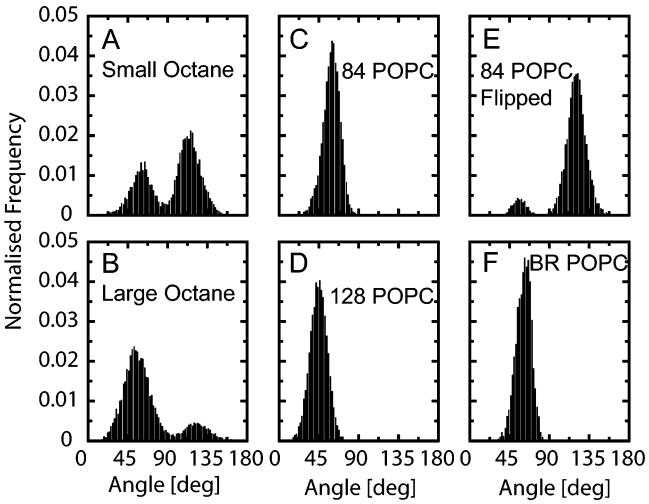

Figure 7. Distribution of the polar θ angles for residue Tyr19. The simulations, as defined in Table 1, are the following: (A) small octane; (B) large octane; (C) 84 POPC; (D) 128 POPC; (E) 84 POPC flipped; and (F) BR POPC.

The most remarkable feature of this analysis is that single-helix simulations seem to accurately retain the orientation of an aromatic ring not only from the complete protein simulations but also from the crystal structure. This is especially intriguing since tilt and kink angles are different for the various systems. Another remarkable result was that the additional orientation of Trp3 sampled in the octane simulations was also found in two of the crystal structures, namely 1ap9 [58] and 1brx.[59]

Only the BR octane simulation results do not agree with any of the other systems, exhibiting different side-chain orientations and no anchoring (data not shown). This is probably due to a difference in the location of the Trp3 residue with respect to the octane−water interface. In the BR octane system the Trp3 residue is fully solvated and ∼0.2 nm away from the octane monolayer surface. Since the helices in the complete bacteriorhodopsin simulations cannot easily tilt or bend the Trp3 residue remains at its initial position, slightly removed from the interface. This explains why no anchoring was observed. This result highlights that one of the main difficulties of octane simulations is presented by the choice of both the slab width and its position with respect to the protein.

Tyr19. Tyr19 is located at the C-terminal interfacial region of helix A. Both the small and large octane simulations sample the initial state from the X-ray structures at $\theta \approx 50°$ and also an additional state at ∼125° (Figure 7). As in the case of Trp3, the POPC simulations only sample the initial state. In the 84 POPC flipped simulations the Tyr19 ring remained in its "new" orientation until ∼9.5 ns when it flipped back toward the original X-ray structure orientation. The bacteriorhodopsin simulations behave like their single-helix counterparts with the BR POPC system exhibiting one peak at the crystallographic angle and

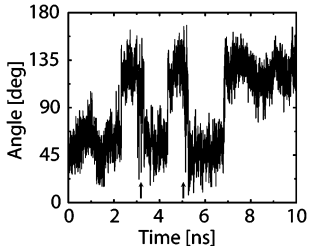

Figure 8. Switch-like time dependence of aromatic ring-flips. The θ angle is shown as a function of time for residue Tyr19 in the small octane system. As indicated by the arrows, at ∼3 and ∼5 ns multiple ring-flips can be seen.

the BR octane system (data not shown) exhibiting two peaks equivalent to those found in the small octane system. Tyr19 has a 50% accessible surface in the X-ray structure and therefore might be expected to have considerable freedom to move.

Note that although the ring flips of Tyr19 at first sight look similar to those in Trp3, in the case of Tyr19 the two states actually have an identical conformation. This is due to the symmetry of the tyrosine side chain. Thus the 90° flip in θ represents a 180° ring flip such that before the flip the OH group is pointing to the CE1 atom. During the ring flip it reorients to point to the CE2 atom.

The time scales of the "flipping" (i.e. the time to switch from one conformation to the other flipped conformation) in POPC are ∼5 ps compared to ∼10−50 ps in octane and follow the switch-like behavior shown in Figure 8. One ring-flip was recorded in POPC compared to an average of seven in the octane simulations. Incidentally one crystallographic structure (1ap9.pdb[58]) shows the Tyr19 residue in the middle of flipping. All the others have similar θ angles of ∼50°. It has been shown by adiabatic free energy calculations that flipping rates (i.e. 180° ring rotations) of tyrosine residues vary between 2×10^{12} s^{-1} and 4×10^{-5} s^{-1} for the four different tyrosines of the bovine pancreatic trypsin inhibitor (BPTI),[60,61] a very small soluble protein. The study showed that the rate of flipping depends strongly on the environment, with the least flipping occurring for buried residues. Tyrosine and phenylalanine residues of BPTI have also been observed by nuclear magnetic resonance.[62,63] The studies found flipping rates ranging between 2 and 10^5 s^{-1} which are substantially lower than the rate estimates from the current simulations which are $\sim 10^9$ s^{-1} for octane. For POPC no estimate was possible since it only flipped once.

The above analysis can be summarized as follows. The intact bacteriorhodopsin simulations in octane and POPC were found to accurately retain the orientation of all flexible aromatic side chains found in the crystal structures. More interestingly the same spatial orientation and behavior was also found for residues Trp3 and Tyr19 in the single-helix simulations, irrespective of the membrane environment.

In general octane simulations seem to present reduced barriers for aromatic ring-flips at the interfaces, thus exploring more conformations. Nevertheless, they were found to sample the same states as the POPC systems. Perhaps the most striking feature of the conformational analysis is that the alignment of aromatics in octane is identical with that in POPC even though the octane membrane has no charges and a substantially different interface. This suggests that although "anchoring" clearly occurs at the membrane−water interface (see below) the conformation of the side chain is determined more by side chain/helix interactions.

Hydrogen Bonding of Aromatic Residues. Having investigated the spatial orientations and dynamics of the aromatics side chains we wish to characterize their interactions at the water/POPC and water/octane interfaces. In Table 4 we compare the hydrogen bonding of Trp3 and Tyr19. For Trp3 the NH group spends roughly 50% of its time hydrogen bonded to water molecules in the octane systems compared to around 38% for the POPC systems. However, the hydrogen bonding with the phosphate oxygen atoms of the POPC lipid headgroups more than compensates for this, increasing the total time spent hydrogen bonded to just over 60%. The time-fraction for more than two hydrogen bonds is less than 4% for both systems indicating that the NH group bonds either to a water or to a headgroup but not to both simultaneously. The decreased hydrogen bonding with water molecules in the POPC systems can be explained by the lower water density at the interfacial regions of the POPC membrane (cf. Figure 1C,D). Nevertheless, the total time spent hydrogen bonding is only marginally increased (by ∼10%) in the POPC systems, since the absence of charged headgroups at the octane membrane interface is compensated for by an increased water density. This might explain why the anchoring is still observed in the octane simulations and also why it is less "strong" in octane. In fact the hydrogen bonding with the lipid headgroups only accounts for one-third of all hydrogen bonds in the POPC system.

Tyr19 displays a slightly different interaction pattern. In the octane systems it spends more than 90% of trajectory time with two or more hydrogen bonds to the water molecules compared to just 45% for the POPC system. Hydrogen bonds with the lipid headgroups compensate for this but unlike Trp3 the total hydrogen bonding is actually stronger in the octane system. This might be due to the location of Tyr19, which is buried more deeply in the POPC membrane (see Figure 1A,B). While it can still interact with the water molecules that have penetrated the membrane beyond the lipid headgroups, it finds itself too far away and shielded from the headgroups itself.

Since the octane slab only mimics the hydrophobic region of the membrane it has a smaller width of ∼3 nm and Tyr19 therefore has contact with the water molecules. However, Figure 1A,B confirms that the location of Tyr19 with respect to the water is roughly the same in both membranes.

Hydrogen Bonding of Charged Residues. It is also of interest to look at the H-bonding interactions of those charged side chains found either side of the TM core of helix A, especially given the discussions of the importance of e.g. lysine side chains in stabilizing helices in a transmembrane orientation.[32,33,64] In Table 5 we summarize the results of hydrogen-bonding analysis for the two charged residues Glu2 and Lys23. For Glu2 the hydrogen bonding with water is again stronger in octane than in the POPC systems with an average of 6 hydrogen bonds in the first and 5 hydrogen bonds in the latter system at any given time. This can again be explained by the reduced water density at the interfaces for the POPC membrane. In the case of Glu2 the lipids cannot compensate for this since both the glutamate side chains and the lipid headgroup contain only H-bond acceptors and hence cannot form hydrogen bonds to one another. There is a minimum of 3 hydrogen bonds at any time in the simulations for both systems indicating a strong interaction with the water.

The hydrogen-bonding distributions of Lys23 with water for both octane and POPC simulations have a very similar shape and both peak at 3 hydrogen bonds. Interestingly, the POPC system has a slightly stronger interaction with the water molecules than octane but hardly any interaction with the POPC lipid headgroups, thus behaving qualitatively like Glu2. This suggests that, at least for helix A, the lysine side chain does

TABLE 4: Aromatic Side Chain H Bonds[a]

	Trp3				Tyr19			
H bonds	water (octane)	water (POPC)	lipid (POPC)	total (POPC)	water (octane)	water (POPC)	lipid (POPC)	total (POPC)
0	50.6	60.0	77.5	37.9	0.1	15.0	62.0	0.4
1	45.6	38.0	21.4	58.7	7.8	39.3	38.0	32.1
2	3.6	2.0	1.1	3.4	70.9	41.8	0.0	62.0
3	0.2	0.0	0.0	0.0	20.9	3.9	0.0	5.5
4	0.0	0.0	0.0	0.0	0.3	0.0	0.0	0.0

[a] The frequency of side chain hydrogen bonds for residues Trp3 and Tyr19 is shown as a percentage of trajectory time for small octane and 84 POPC simulations. Results for the other systems are similar. Hydrogen bond analysis was performed geometrically: the donor−hydrogen−acceptor angle had to be less than 60° and the hydrogen−acceptor distance less than 0.25 nm.

TABLE 5: Charged Side Chain H Bonds[a]

	Glu2		Lys23			
H bonds	water (octane)	water (POPC)	water (octane)	water (POPC)	lipid (POPC)	total (POPC)
0	0.0	0.0	0.0	0.0	97.9	0.0
1	0.0	0.0	1.7	0.1	2.1	0.0
2	0.0	0.0	16.1	6.6	0.0	5.6
3	0.8	4.6	62.6	76.1	0.0	76.4
4	9.3	28.0	17.9	16.5	0.0	17.2
5	28.7	36.4	1.7	0.7	0.0	0.8
6	34.0	24.7				
≥7	27.2	6.3				

[a] The frequency of hydrogen bonds for residues Glu3 and Lys23 is shown as a percentage of trajectory time for small octane and 84 POPC simulations. Results for the other systems are similar. Note that H bonds between a glutamate side chain and a POPC headgroup are not possible as neither group contains any H-bond donors.

indeed "snorkel" up to the water molecules to H bond with them.[65] Thus basic side chains, e.g., lysine, prefer to interact with water molecules in the interface and amphipathic aromatic residues, e.g., tryptophan, interact with both lipid headgroups and water molecules in the interface.[56,32]

Electrostatic Interactions. The electrostatic interactions of helix A with water and with the membrane are summarized in Table 6. If the above findings for aromatics and charged side chains are correct the interaction energy for the POPC systems should be roughly the same as that for the octane systems. In other words, an increased water−protein interaction should compensate for the polar headgroups at the octane−membrane interface. Indeed this seems to be the case. For both the small and the large systems, the total interaction energy is only ∼10% larger for a POPC than for an octane membrane. Thus the interactions of helix A in the octane membrane provide a good energetic mimic of those in the POPC membrane.

Interactions with Solvent. Helix A of bacteriorhodopsin has a net dipole of 238 debye such that the N-terminus is ca. $-^2/_3$ e and the C-terminus is ca. $+^2/_3$ e. This net dipole is composed of the usual α-helix backbone dipole moment [66,67] (which on its own would result in ca. +0.5 e at the N-terminus and ca. −0.5 e at the C-terminus) in addition to two charged residues (Glu2 and Lys23) that cancel and reverse the backbone dipole. The net dipole moment thus created is approximately parallel to the backbone dipole. As there has been some interest in the possible roles of TM helix dipoles in membrane protein function[68−70] it is of interest to examine the effect of the helix A dipole on the orientation of water molecules in the adjacent solvent regions.

Figure 9 shows the effect of the dipole moment on the surrounding water molecules. The electric field lines due to the charges at the termini can clearly be seen. A comparison between the average alignment of water molecules for the last 0.8 ns of the 1 ns equilibration runs in the water and octane slab simulations produce similar water alignments outside the membrane region. The correlation of the water alignment with the local electric field is very high with a time average of ∼90% of water molecules aligned with the local field to within a few degrees. The octane simulations show that even though helix A possesses a strong dipole moment the field caused by it is nevertheless of quite short range. In fact most of the water ordering is no further than 0.5 nm away from the helix termini. Repeating the octane simulation with Ewald summation rather than the 1.8 nm electrostatic cutoff gives slightly decreased alignment of the water dipoles, especially at the box boundaries.

The POPC simulations produce much stronger alignment due to the significant dipoles of the lipid headgroups. The field lines can be seen to cross the simulation box boundaries (*z*-axis) indicating that the ordering effect has a long range. This has been suggested to lead to possible artifacts in, e.g., simulations of alamethicin channels.[71]

Discussion

In the context of understanding the structure and stability of membrane proteins, the value of simulation studies is that they enable us to explore the role of *environment* in determining the conformational dynamics of integral membrane proteins and their domains. This is of some relevance given the use of nonaqueous solvent systems,[72−76] of detergent micelles,[77−80] and of detergent-containing crystals[81,82] in experiments to determine the structures of membrane proteins. Simulations can provide information on the relationship between conformational dynamics and environment[83] to facilitate extrapolation from in vitro environments to the in vivo environment. To exploit such simulations, it is important that we understand the effects of choice of the membrane mimetic environment and of simulation protocol on the outcome of a simulation.

The two membranes used in the presented simulations are different in a number of features. POPC has strongly polar interfaces with higher density than the membrane interior. The water molecules in the vicinity and even at nanometer distances from these interfaces are strongly aligned with the local electric field of the polar headgroups and their rate of random diffusion is significantly decreased. In comparison the octane interfaces are simple, with no decreased density, and the water molecules have bulk properties all the way to the interface. Nevertheless, it appears that the only major difference in the simulations is that the sampling of the protein or helix in octane is faster and more conformational space is explored. Both are desirable properties in computer simulations of biomolecules as long as the sampling is confined to the states that the protein samples in nature. The only way to test that is by comparing the simulation results to the thermodynamic and structural data available through theory and experiment. However, simulations found differences in tilt and kink angle distributions between

TABLE 6: Electrostatic Interaction Energies[a]

	water		POPC		
system	short range	long range	short range	long range	total
small octane	−1067(±89)	−127(±32)			−1194
84 POPC	−980(±113)	−16(±30)	−319(±238)	+65(±234)	−1250
large octane	−1051(±98)	−119(±34)			−1170
128 POPC	−888(±122)	−3.7(±35)	−384(±204)	−121(±240)	−1397

[a] Electrostatic interaction energies in kcal/mol, split into a short-range and a long-range contribution, for the interaction of helix A with the membrane and water. The total interaction energy with the surroundings is given in the last column. Octane is neutral and hence does not contribute to the electrostatic interaction.

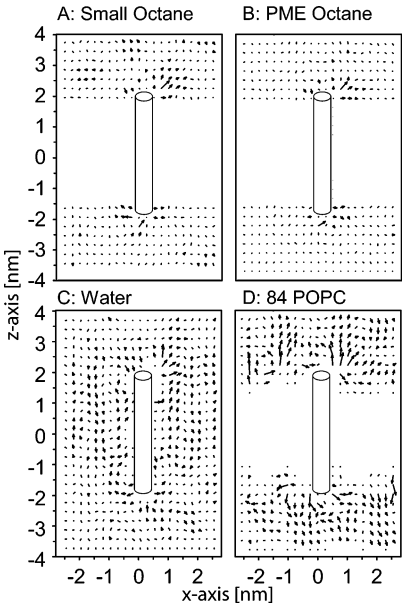

Figure 9. Orientation of water dipoles. The average orientation of water dipoles averaged over 0.8 ns was calculated for various simulation conditions. Effects of the helix dipole on the orientation of water molecules were calculated by dividing the solvent space into a grid and calculating the time averaged electric dipole for each grid cell. This analysis was for the latter 0.8 ns of the 1 ns equilibration runs during which the helix was held in place by harmonic restraints to all atoms. The position of the helix, as indicated by the cylinder, is such that its N-terminus is uppermost. Note that the presence of the charged side chains Glu2 and Lys23 imparts a net dipole of ∼240 D oriented such that the N-terminus of the helix is negative and the C-terminus positive. In panels A and B a comparison is shown for the small octane system, using either (A) a cutoff or (B) Ewald summation to treat long-range interactions. The bottom panels show a comparison between (C) the water and (D) 84 POPC simulations.

larger and smaller systems. These can be attributed to differences in membrane rigidity. Periodic boundary conditions force systems with decreasing size into increasingly flat membrane configurations. Simulations of lipid bilayer membranes have demonstrated considerable surface curvature for larger systems.[84] The question remains which systems are more realistic. This will ultimately depend on the rigidity of membranes in vivo and will most likely be dependent on a range of other factors such as protein−lipid ratio as well as lipid composition. Nevertheless, tilt, kink, and essential dynamics analysis showed that the dynamics in both octane and POPC single-helix systems are very similar. The only simulations that differ in the dynamics are the intact protein simulations. This was to be expected since single-helix simulations by nature exclude protein−protein interactions, which will play an important role in the dynamics of the protein fragments.

A key question for membrane proteins is how they maintain their inserted orientation in a membrane that is in constant motion. One hypothesis proposes that aromatics play a key role by acting as anchors.[32,56,85] In support of this proposal, conformational stabilization of the aromatic residues at the membrane−water interfaces was found in all of the current simulations. Although the side chains sample virtually all possible orientations in the simulations they nevertheless exhibit a very strong preference for specific orientations. This suggests that the interfacial environment limits the orientational space available for aromatic side chains. The most remarkable property was that the conformations sampled were not only identical between all simulations but also coincided with the conformations found in the X-ray structures. In the case of Trp3 a conformational state was sampled in octane that was found independently in two crystal structures. This suggests that helices can anchor in the membrane individually and assume native state side-chain conformations, in direct support of the two-stage membrane folding model suggested by Popot and Engelman.[18,19,86] One other remarkable result of the analysis is that the charged lipid headgroups are not required to observe this anchoring process. In fact the current analysis suggests that the electrostatic interaction of the aromatics may be mainly with the water molecules, whose bulk presence at the octane−water interface compensates for the lack of charges and dipoles. Further comparative simulation studies will be required to see whether this is true for all membrane proteins.[87]

Experimentally helix A has been found to adopt a stable predominantly α-helical conformation in SDS.[23,24] The α-helical content was virtually unchanged by transfer to phospholipid vesicles. Both circular dichroism and Fourier transform infrared spectroscopy showed virtually identical behavior of isolated helix A compared to intact bacteriorhodopsin suggesting that in the phospholipid vesicles helix A adopts a stable transmembrane orientation. Protease protection experiments on vesicles in solution showed that helix A is the most strongly protected from digestion.[23,24] In the current computational study helix A remained stable in all simulations. Indeed, even in water it was found to be remarkably stable retaining much of its helicity throughout the duration of the simulations. Tilt and kink angles, RMSD values, RMSF profiles, essential dynamics, and even aromatic ring orientations all suggest that the data for single-helix simulations are complementary to the complete protein simulations. The essential dynamics data suggest that the sampling of motion is much decreased in the full protein simulations compared to that in their single-helix counterparts. Helix A has a substantial dipole moment that aligns water molecules at its termini, although the alignment was shown to be of short range. Differences in parameters were shown to be largely insignificant with the particle mesh Ewald method showing essentially identical behavior at nearly twice the computational time. On the other hand, heavy hydrogen and dummy atoms decrease the computer time required by half (because they allow a larger time step) while still producing nearly identical data. In fact the only substantial difference found when using heavy hydrogen and dummy atoms was in the

behavior of Trp3, which suggests that for aromatics at the interfaces this method might not be optimal.

In summary, the choice of membrane mimetic seems to have only a small effect on the equilibrium dynamics and conformation of a single α-helical transmembrane peptide. Surprisingly the very simplified interface of the octane membrane still captures most of the essential properties of the POPC membrane. Hydrogen bonding of aromatics and charged groups at the interface of the POPC membrane is compensated for by increased interactions with water in the octane system and the electrostatic interaction energies were found to be very similar.

Acknowledgment. Work in the group of MSP Sansom is supported by the Wellcome Trust, BBSRC and EPSRC. M.B.U. was supported by the MRC, and is now a Wellcome Trust Travelling Fellow. D.P.T. is a Scholar of the Alberta Heritage Foundation for Medical Research. Work in D.P.T.'s group is supported by the Canadian Institutes of Health Research. We thank the Oxford super computer center (OSC) for computer time.

References and Notes

(1) Lanyi, J. K.; Luecke, H. *Curr. Opin. Struct. Biol.* **2001**, *11*, 415.
(2) Woolf, T. B. *Biophys. J.* **1997**, *73*, 2376.
(3) Woolf, T. B. *Biophys. J.* **1998**, *74*, 115.
(4) Logunov, I.; Humphrey, W.; Schulten, K.; Sheves, M. *Biophys. J.* **1995**, *68*, 1270.
(5) Hermone, A.; Kuczera, K. *Biochemistry* **1998**, *37*, 2843.
(6) Simon, C.; Aalouach, M.; Smith, J. C. *Faraday Discuss.* **1998**, *111*, 95.
(7) Hermone, A.; Kuczera, K. *Biochemistry* **1998**, *37*, 2843.
(8) Baudry, J.; Crouzy, S.; Roux, B.; Smith, J. C. *Biophys. J.* **1999**, *76*, 1909.
(9) Tajkhorshid, E.; Baudry, J.; Schulten, K.; Suhai, S. *Biophys. J.* **2000**, *78*, 683.
(10) Warshel, A.; Chu, Z. T. *J. Phys. Chem. B* **2001**, *105*, 9857.
(11) Rajamani, R.; Gao, J. L. *J. Comput. Chem.* **2002**, *23*, 96.
(12) Shen, L.; Bassolino, D.; Stouch, T. *Biophys. J.* **1997**, *73*, 3.
(13) Belohorcova, K.; Davis, J. H.; Woolf, T. B.; Roux, B. *Biophys. J.* **1997**, *73*, 3039.
(14) Petrache, H. I.; Grossfield, A.; MacKenzie, K. R.; Engelman, D. M.; Woolf, T. B. *J. Mol. Biol.* **2000**, *302*, 727.
(15) Law, R. J.; Forrest, L. R.; Ranatunga, K. M.; La Rocca, P.; Tieleman, D. P.; Sansom, M. S. P. *Proteins*: *Struct. Funct. Genet.* **2000**, *39*, 47.
(16) Saiz, L.; Klein, M. L. *Acc. Chem. Res.* **2002**, *35*, 482.
(17) Lopez, C. F.; Montal, M.; Blasie, J. K.; Klein, M. L.; Moore, P. B. *Biophys. J.* **2002**, *83*, 1259.
(18) Popot, J. L.; Engelman, D. M. *Biochemistry* **1990**, *29*, 4031.
(19) Popot, J. L.; Engelman, D. M. *Annu. Rev. Biochem.* **2000**, *69*, 881.
(20) Pervushin, K. V.; Arseniev, A. S. *FEBS Lett.* **1992**, *308*, 190.
(21) Lomize, A. L.; Pervushkin, K. V.; Arseniev, A. S. *J. Biomol. NMR* **1992**, *2*, 361.
(22) Barsukov, I. L.; Nolde, D. E.; Lomize, A. L.; Arseniev, A. S. *Eur. J. Biochem.* **1992**, *206*, 665.
(23) Hunt, J. F.; Earnest, T. N.; Bousche, O.; Kalghatgi, K.; Reilly, K.; Horvath, C.; Rothschild, K. J.; Engelman, D. M. *Biochemistry* **1997**, *36*, 15156.
(24) Hunt, J. F.; Rath, P.; Rothschild, K. J.; Engelman, D. M. *Biochemistry* **1997**, *36*, 15177.
(25) Katragadda, M.; Alderfer, J. L.; Yeagle, P. L. *Biophys. J.* **2001**, *81*, 1029.
(26) Schiffer, M.; Chang, C. H.; Stevens, F. J. *Protein Eng.* **1992**, *5*, 213.
(27) Yau, W. M.; Wimley, W. C.; Gawrisch, K.; White, S. H. *Biochemistry* **1998**, *37*, 14713.
(28) Grossfield, A.; Woolf, T. B.; Pearson, J. G. *Int. J. Quantum Chem.* **1999**, *75*, 197.
(29) Grossfield, A.; Woolf, T. B. *Langmuir* **2002**, *18*, 198.
(30) Ulmschneider, M. B.; Sansom, M. S. P. *Biochim. Biophys. Acta* **2001**, *1512*, 1.
(31) Lee, A. G. *Biochim. Biophys. Acta* **2003**, *1612*, 1.
(32) Killian, J. A.; von Heijne, G. *Trends Biochem. Sci.* **2000**, *25*, 429.
(33) de Planque, M. R. R.; Killian, J. A. *Mol. Membr. Biol.* **2003**, *20*, 271.
(34) Petrache, H. I.; Zuckerman, D. M.; Sachs, J. N.; Killian, J. A.; Koeppe, R. E.; Woolf, T. B. *Langmuir* **2002**, *18*, 1340.
(35) Sass, H. J.; Buldt, G.; Gessenich, R.; Hehn, D.; Neff, D.; Schlesinger, R.; Berendzen, J.; Ormos, P. *Nature* **2000**, *406*, 649.
(36) Tieleman, D. P.; Sansom, M. S. P.; Berendsen, H. J. C. *Biophys. J.* **1999**, *76*, 40.
(37) Faraldo-Gómez, J.; Smith, G. R.; Sansom, M. S. P. *Eur. Biophys. J.* **2002**, *31*, 217.
(38) Ulmschneider, M. B.; Tieleman, D. P.; Sansom, M. S. P. Manuscript in preparation.
(39) Spassov, V. Z.; Luecke, H.; Gerwert, K.; Bashford, D. *J. Mol. Biol.* **2001**, *312*, 203.
(40) Nina, M.; Roux, B.; Smith, J. C. *Biophys. J.* **1995**, *68*, 25.
(41) Berendsen, H. J. C.; van der Spoel, D.; van Drunen, R. *Comput. Phys. Commun.* **1995**, *95*, 43.
(42) van Gunsteren, W. F.; Kruger, P.; Billeter, S. R.; Mark, A. E.; Eising, A. A.; Scott, W. R. P.; Huneberger, P. H.; Tironi, I. G. *Biomolecular Simulation*: *The GROMOS96 Manual and User Guide*; Biomos & Hochschulverlag AG an der ETH Zurich: Groningen and Zurich, Switzerland, 1996.
(43) Berendsen, H. J. C.; Postma, J. P. M.; van Gunsteren, W. F.; Hermans, J. *Intermolecular Forces*; Reidel: Dordrecht, The Netherlands, 1981.
(44) Berger, O.; Edholm, O.; Jahnig, F. *Biophys. J.* **1997**, *72*, 2002.
(45) Berendsen, H. J. C.; Postma, J. P. M.; van Gunsteren, W. F.; DiNola, A.; Haak, J. R. *J. Chem. Phys.* **1984**, *81*, 3684.
(46) Hess, B.; Bekker, H.; Berendsen, H. J. C.; Fraaije, J. G. E. M. *J. Comput. Chem.* **1997**, *18*, 1463.
(47) Feenstra, K. A.; Hess, B.; Berendsen, H. J. C. *J. Comput. Chem.* **1999**, *20*, 786.
(48) Darden, T.; York, D.; Pedersen, L. *J. Chem. Phys.* **1993**, *98*, 10089.
(49) Essmann, U.; Perera, L.; Berkowitz, M. L.; Darden, T.; Lee, H.; Pedersen, L. G. *J. Chem. Phys.* **1995**, *103*, 8577.
(50) VanAalten, D. M. F.; DeGroot, B. L.; Findlay, J. B. C.; Berendsen, H. J. C.; Amadei, A. *J. Comput. Chem.* **1997**, *18*, 169.
(51) Amadei, A.; Linssen, A. B. M.; Berendsen, H. J. C. *Proteins*: *Struct. Funct. Genet.* **1993**, *17*, 412.
(52) Hess, B. *Phys. Rev. E* **2000**, *62*, 8438.
(53) Wiener, M. C.; White, S. H. *Biophys. J.* **1992**, *61*, 434.
(54) Bowie, J. U. *J. Mol. Biol.* **1997**, *272*, 780.
(55) Kabsch, W.; Sander, C. *Biopolymers* **1983**, *22*, 2577.
(56) de Planque, M. R. R.; Kruijtzer, J. A. W.; Liskamp, R. M. J.; Marsh, D.; Greathouse, D. V.; Koeppe, R. E.; de Kruijff, B.; Killian, J. A. *J. Biol. Chem.* **1999**, *274*, 20839.
(57) Forrest, L. R.; Sansom, M. S. P. *Curr. Opin. Struct. Biol.* **2000**, *10*, 174.
(58) Pebay-Peyroula, E.; Rummel, G.; Rosenbusch, J. P.; Landau, E. M. *Science* **1997**, *277*, 1676.
(59) Luecke, H.; Richter, H. T.; Lanyi, J. K. *Science* **1998**, *280*, 1934.
(60) Gelin, B. R.; Karplus, M. *Proc. Natl. Acad. Sci. U.S.A.* **1975**, *72*, 2002.
(61) Gelin, B. R.; Karplus, M. *J. Am. Chem. Soc.* **1975**, *97*, 6996.
(62) Skalicky, J. J.; Mills, J. L.; Sharma, S.; Szyperski, T. *J. Am. Chem. Soc.* **2001**, *123*, 388.
(63) Nall, B. T.; Zuniga, E. H. *Biochemistry* **1990**, *29*, 7576.
(64) Strandberg, E.; Killian, J. A. *FEBS Lett.* **2003**, *544*, 69.
(65) Mishra, V.; Palgunachari, M.; Segrest, J.; Anantharamaiah, G. *J. Biol. Chem.* **1994**, *269*, 7185.
(66) Wada, A. *Adv. Biophys.* **1976**, *9*, 1.
(67) Hol, W. G. J.; van Duijnen, P. T.; Berendsen, H. J. C. *Nature* **1978**, *273*, 443.
(68) Mathew, M. K.; Balaram, P. *FEBS Lett.* **1983**, *157*, 1.
(69) Edmonds, D. T. *Eur. Biophys. J.* **1985**, *13*, 31.
(70) Kienker, P. K.; DeGrado, W. F.; Lear, J. D. *Proc. Natl. Acad. Sci. U.S.A.* **1994**, *91*, 4859.
(71) Bostick, D. L.; Berkowitz, M. L. *Biophys. J.* **2003**, *85*, 97.
(72) Sessions, R. B.; Gibbs, N.; Dempsey, C. E. *Biophys. J.* **1998**, *74*, 138.
(73) Chambers, E. J.; Bloomberg, G. B.; Ring, S. M.; Tanner, M. J. A. *J. Mol. Biol.* **1999**, *285*, 1289.
(74) Girvin, M. E.; Rastogi, V. K.; Abildgaard, F.; Markley, J. L.; Fillingame, R. H. *Biochemistry* **1998**, *37*, 8817.
(75) Rastogi, V. K.; Girvin, M. E. *Nature* **1999**, *402*, 263.
(76) Dmitriev, O. Y.; Abildgaard, F.; Markley, J. L.; Fillingame, R. H. *Biochemistry* **2002**, *41*, 5537.
(77) Arora, A.; Abildgaard, F.; Bushweller, J. H.; Tamm, L. K. *Nat. Struct. Biol.* **2001**, *8*, 334.
(78) Tamm, L. K.; Abildgaard, F.; Arora, A.; Blad, H.; Bushweller, J. H. *FEBS Lett.* **2003**, *555*, 139.
(79) Fernandez, C.; Hilty, C.; Bonjour, S.; Adeishvili, K.; Pervushin, K.; Wuthrich, K. *FEBS Lett.* **2001**, *504*, 173.

(80) Fernandez, C.; Wüthrich, K. *FEBS Lett.* **2003**, *555*, 144.
(81) Pautsch, A.; Vogt, J.; Model, K.; Siebold, C.; Schulz, G. E. *Proteins*: *Struct. Funct. Genet.* **1999**, *34*, 167.
(82) Pautsch, A.; Schulz, G. E. *J. Mol. Biol.* **2000**, *298*, 273.
(83) Bond, P.; Sansom, M. S. P. *J. Mol. Biol.* **2003**, *329*, 1035.
(84) Lindahl, E.; Edholm, O. *Biophys. J.* **2000**, *79*, 426.
(85) Killian, J. A. *FEBS Lett.* **2003**, *555*, 134.
(86) Engelman, D. M.; Chen, Y.; Chin, C.; Curran, R.; Dixon, A. M.; Dupuy, A.; Lee, A.; Lehnert, U.; Mathews, E.; Reshetnyak, Y.; Senes, A.; Popot, J. L. *FEBS Lett.* **2003**, *555*, 122.
(87) Domene, C.; Bond, P. J.; Deol, S. S.; Sansom, M. S. P. *J. Am. Chem. Soc.* **2003**, *125*, 14966.